MSDE



COMMUNICATION

View Article Online



Cite this: *Mol. Syst. Des. Eng.*, 2021, **6**, 708

Received 29th June 2021, Accepted 26th July 2021

DOI: 10.1039/d1me00082a

rsc.li/molecular-engineering

Improving high rate cycling limitations of thick sintered battery electrodes by mitigating molecular transport limitations through modifying electrode microstructure and electrolyte conductivity†

Ziyang Nie,^a Rohan Parai,^b Chen Cai,^a Dipankar Ghosh ^{10 b} and Gary M. Koenig Jr. ^{10 *a}

For batteries, thicker electrodes increase energy density, however, molecular transport limits the rate of charge/discharge for extracting large fractions of available energy. Mitigating transport limitations by increasing electrolyte conductivity and aligning the pores in the electrode microstructure are described.

Introduction

Lithium-ion (Li-ion) batteries have received great research interest due to their relatively high energy and power density.1,2 Although Li-ion batteries have been successfully commercialized and used in many applications, further improvements are still necessary as energy storage demands are ever increasing.3,4 Often gains are made in energy and power density though new electrode materials or cell chemistry.⁵⁻⁹ However, improvements in desired cell properties can also be achieved by engineering the electrode structure and/or using electrolytes with different transport characteristics. 10-12 Commercial Li-ion batteries composite electrodes. These thin film (typically $<100 \mu m$)¹³ composites are coated on metal current collectors and consist of active material that undergoes electrochemical reactions, conductive additives to improve electronic conductivity and polymer binders to maintain the electrode integrity. 14,15 Therefore, at the cell level, increasing electrode thickness and reducing inactive additives are routes to increase energy density. However, the inactive components in composite electrode pores greatly increase tortuosity and restrict ion transport at increased thicknesses. 16 One alternative

Design, System, Application

Lithium-ion batteries are a leading energy storage technology. Sintered electrodes which have greater electrode thickness than conventional composite electrodes and do not contain any carbon or polymer additives have recently been reported. The sintered electrodes can achieve high energy density at the system level due to increased thickness, and the lack of additives may improve molecular transport properties by removing inactive components from the interstitial region between electroactive particles which is filled with electrolyte. However, the sintered electrodes are limited in their rate of charge/ discharge by molecular transport resistances due to their thick structure. This work applied two design strategies to mitigate the molecular transport limitation: modifying the electrolyte composition (to change ionic conductivity) and aligning the microstructure of one of the battery electrodes. These designs were pursued in isolation and combination, and improved the ability to deliver electrochemical energy at increasing rates. These results demonstrate to researchers design strategies to pursue improved high energy density batteries with thick electrodes. This design framework is valuable more generally for electrochemical systems where the molecular transport in the liquid phase is a limitation.

electrode architecture recently explored includes only electroactive material free of additives, which undergoes a heat treatment to improve the mechanical strength of the porous pellet. These will be referred to as "sintered" electrodes, and such processing has been used to fabricate relatively thick electrodes, in some cases exceeding 1500 $\mu m.^{17-19}$

While sintered electrodes do not have inactive components in the interstitial regions between electroactive particles, the electrodes are still very thick and thus previous reports have suggested the long molecular transport path length for Li⁺ through the microstructure limits the ability to achieve high active material utilization (*e.g.*, capacity) and high rates of charge/discharge.^{20,21} To mitigate this liquid phase ion transport limitation while maintaining thick and high energy density electrodes, there are two main routes to

^a Department of Chemical Engineering, University of Virginia, 102 Engineers Way, Charlottesville, 22904-4741, VA, USA. E-mail: gary.koenig@virginia.edu

^b Department of Mechanical and Aerospace Engineering, Old Dominion University, Norfolk, 23529, VA, USA

 $[\]dagger$ Electronic supplementary information (ESI) available. See DOI: 10.1039/ d1me00082a

MSDE Communication

pursue: engineer the electrode microstructure to facilitate improved molecular transport, 22-24 or modify the molecular composition of the electrolyte to use an electrolyte with higher ionic conductivity (and/or Li⁺ transference number).^{25,26} From an electrode microstructure standpoint, typically the goal is to process electrodes such that the pores are aligned in the direction of net Li⁺ flux during charge/ discharge, such that the tortuosity is reduced and mass transport limitations are alleviated. To achieve such engineered microstructures (both for sintered and composite electrodes), techniques have included templating pores/voids using ice, 22 magnetic fields 23 and wood. 24 Higher electrolyte conductivity, and in some cases concentration, can also mitigate Li⁺ transport limitations through the electrode microstructure and facilitate faster charge/discharge for battery electrodes in general.²⁷ In previous publications, hydraulically pressed and sintered LiCoO2 (LCO) cathodes and Li₄Ti₅O₁₂ (LTO) anodes were cycled in battery cells and transport processes were inferred using electrochemical and imaging measurements combined neutron simulations. 20,28 Recently, the advantages of ice-templated sintered electrodes with regards to rate capability (and speculated to result from improved transport through the electrode microstructure) were reported.²² In this work, the impact of higher ionic conductivity electrolytes, in isolation and in combination with ice-templating to facilitate aligning the pores/voids in the electrode microstructure, on the retention of capacity at increasing rates of charge/discharge for sintered electrode LTO/LCO full cells will be reported. As the thick sintered electrodes have been reported to be limited by the process of ion transport through the electrode microstructure, both the microstructure templating and change in electrolyte were expected to improve the rate capability of the cells, and the effects of these changes in isolation and combination will be reported and were found to be substantive.

Results and discussion

As mentioned earlier, the capacity retention for thick sintered electrodes at increasing charge/discharge rates and current densities (i.e., rate capability) has for many cases been reported to be limited by Li⁺ transport through the electrolyte-laden porous electrode microstructure. One way to improve on Li⁺ transport limitations is to change the electrolyte used in the cell to increase the ionic conductivity. For this study, the electrolyte investigated contained lithium bis(fluorosulfonyl)imide (LiFSI) as the primary salt dissolved in dimethyl carbonate (DMC). LiFSI was chosen as it has previously been investigated as an electrolyte for high rate battery applications, 29,30 and DMC was chosen as it has relatively low viscosity.^{25,26} Factors such as electrolyte viscosity and its interactions with the electrode components (e.g., wetting and contact angle) have previously been demonstrated as important for electrolyte transport properties. 26,29,31 LiPF $_6$ at 0.5 mol L $^{-1}$ was also added to all

Table 1 Composition of LiFSI-based electrolytes used

| Electrolyte | $\mathrm{Li^{\scriptscriptstyle{+}}}$ concentration (mol $\mathrm{L^{\scriptscriptstyle{-1}}}$) | LiFSI: LiPF ₆ (mol: mol) |
|-------------|--|-------------------------------------|
| HIGH | 2.5 | 6:1 |
| PEAK | 2.0 | 4:1 |
| LOW | 1.3 | 2:1 |
| | | |

LiFSI electrolytes, to mitigate any potential corrosion of the current collector. A LiPF₆-based commercial electrolyte (denoted in this work as GEN2, which was 1.2 mol L⁻¹ LiPF₆ in 3:7 (w/w) ethylene carbonate (EC)/ethyl methyl carbonate (EMC)) was also used as a baseline comparison, and its conductivity as a function of LiPF₆ molarity can be found in ESI,† Fig. S1.32 The LiFSI-based electrolyte compositions used in this study can be found in Table 1. The ionic conductivity as a function of concentration for the three different LiFSI: LiPF₆ ratios used can be found in Fig. 1. The blue dots in Fig. 1 correspond to the locations for the total Li+ concentrations and measured ionic conductivities for the three electrolytes. The electrolytes are referred to as HIGH (the highest concentration of the three, 2.5 mol L⁻¹ Li⁺ and 6:1 LiFSI: LiPF₆), LOW (the lowest concentration of the three, 1.3 mol L⁻¹ Li⁺ and 2:1 LiFSI:LiPF₆), and PEAK (located near the peak in ionic conductivity, with 2.0 mol L^{-1} Li⁺ and 4:1 LiFSI: LiPF₆). Additional experimental details on electrolyte preparation can be found in ESI† (including ref. 33 and 34). The measured conductivity as a function of Li concentration was similar for the 3 different FSI-: PF₆ ratios, although the electrolyte with the higher relative PF6 concentration was slightly lower at a given Li⁺ molarity. Overall, the conductivities were similar to previous reports for pure LiFSI in DMC solution.²⁹

To evaluate impact of the different electrolytes on rate capability of sintered electrode full cells, coin cells were fabricated where the only difference was the electrolyte used (PEAK, LOW, HIGH, or GEN2). Details of the electrode material and electrode fabrication can be found in ESI† and

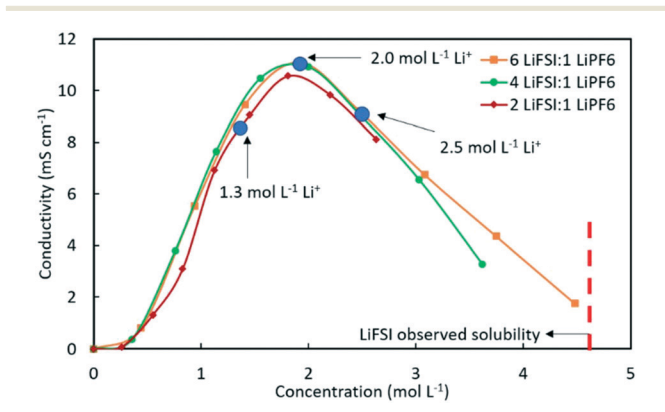


Fig. 1 Ionic conductivity as a function of total Li⁺ concentration for molar ratios of LiFSI:LiPF₆ salt added of 6:1 (orange squares), 4:1 (green circles), and 2:1 (red diamonds). Lines added to guide the eye. The three LiFSI-based electrolytes used in this study are indicated at the blue circle locations. The observed solubility for LiFSI is noted at the concentration where there is a vertical red dashed line.

MSDE Communication

in previous publications. 20,22,28,35-38 The LTO anodes were approximately 0.19 g, 900 µm thick, and had a geometric porosity/void volume fraction of 55%; the LCO cathodes were approximately 0.19 g, 450 µm thick and had a geometric porosity/void volume fraction of 40%. It is noted that lower pore volume fractions would be desirable to increase electrode and cell energy density, especially for the LTO; however, the LTO porosity was near the limit of what was achievable for the slurry conditions used for the freezecasting process to direct the microstructure. The geometric area of the all electrodes was ~1.33 cm², and the reversible low rate (C/50 charge and discharge, or 0.43 mA cm⁻²) capacity for all cells was similar (ranging 123 to 129 mA h g⁻¹ LCO, or 23.5 to 24.6 mA h). For all cells, after initial slow cycling at C/50 charge/discharge, rate capability was performed by charging at C/20 and discharging at the indicated rate with the discharge capacity retention noted in Fig. 2a for the indicated electrolytes (discharge capacity on a total and LCO gravimetric bases can be found in ESI,† Fig. S2). Each cycling data point was averaged from outcomes of 5 cycles at each rate for at least two nominally identical cells for each electrode-electrolyte combination.

For Fig. 2a, the discharge capacity retention was relative to the capacity delivered at C/20 discharge. As is generally the case, the discharge capacity was reduced as the rate of discharge increased, and C/20 cycling after the rate capability testing ("C/20*" in Fig. 2a) indicated capacity losses were not due to capacity fade but were consistent with other processes within the cell limiting achievable capacity at increasing rate/ current density. Further evidence supporting cycling stability was through cycle life testing of sintered LTO/LCO cells with GEN2 and PEAK electrolyte (ESI,† Fig. S3). After the rate capability testing, the capacity retention for an additional 100 cycles for both GEN2 and PEAK cells was above 90%. The discharge capacities for the different electrolytes started to separate even at C/10, and at C/5 and C/2.5 it became clear that the order of rate capability for the cells was PEAK > HIGH > GEN2 > LOW from the best to the worst. With regards to the three LiFSI-based electrolytes, the rate capability outcomes were consistent with ion conduction through the electrolyte being the rate limiting process. The PEAK electrolyte had the highest initial conductivity, consistent with the highest rate capability if Li⁺ transport was the limiting process. In addition, during discharge Li+ deintercalated from the LTO solid phase, traversed to the cathode via the liquid electrolyte, and intercalated into the LCO solid phase. This resulted in a concentration gradient in the electrolyte where there was a relatively high concentration of Li⁺ in regions where reactions were occurring in the LTO anode and a relatively low concentration of Li⁺ in regions where reactions were occurring in the LCO cathode. 20,28 Thus, there were gradients in concentration (and conductivity) throughout the cell depth and areas of extreme depletion would result in polarization that results in reaching the cut off voltage and ending the discharge. From the initial conductivity/concentration point for PEAK, there was a

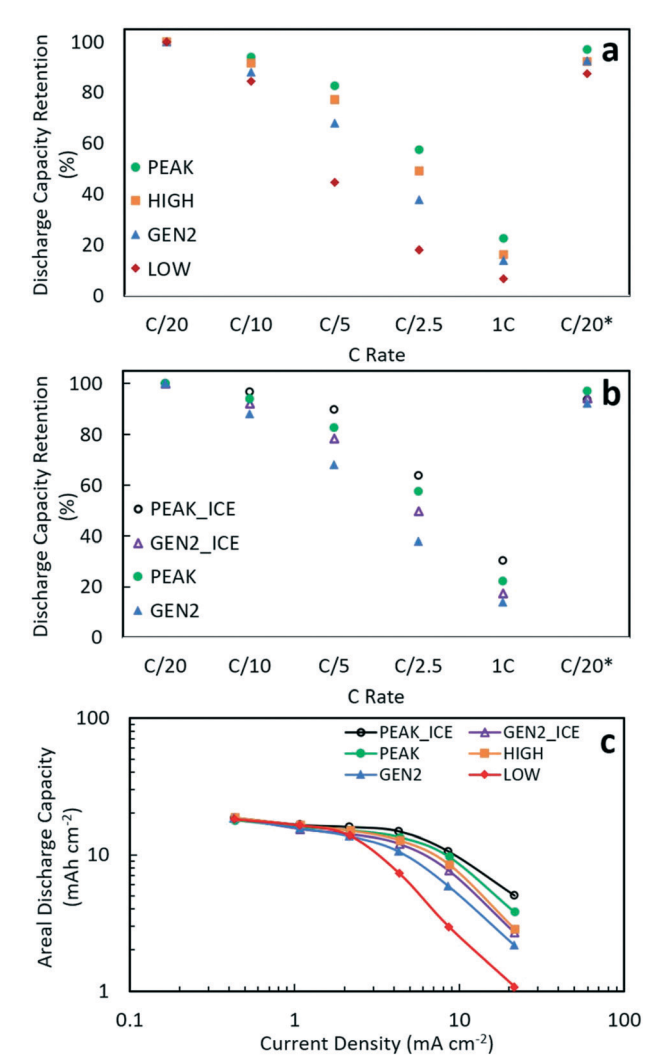


Fig. 2 (a) Discharge capacity retention at the indicated different discharge rates for LTO/LCO sintered cells containing the electrolytes described in the text and Table 1: PEAK (green circles), HIGH (orange squares), LOW (red diamonds), and GEN2 (blue triangles). (b) Discharge capacity retention at the indicated different discharge rates for LTO/ LCO sintered cells containing the electrolytes PEAK and GEN2, where the cases where the LTO was ice-templated and paired with the PEAK (black border circle) and GEN2 (purple border triangle) have been added. (c) Areal discharge capacity delivered as a function of current density for all cells in this report, where the symbols correspond to the same cells as described in (a) and (b). For (a) and (b), all charge cycles were at C/20, and the * represents C/20 discharge cycles after the rate capability test was completed. For (c), lines have been added to guide the eye.

significant buffer in either direction of Li⁺ concentration of relatively high conductivity, which would help with retaining rate capability for a large concentration gradient due to high Li⁺ flux at high rate. The influence of the likely effect of concentration gradient that develops during discharge was more pronounced for LOW and HIGH, where the as-prepared ionic conductivities were similar, but where in regions of Li⁺ depletion during discharge the LOW conductivity will drop much faster than the HIGH conductivity drops for regions where the Li⁺ concentration was increasing (and much bigger

MSDE Communication

Li⁺ concentration swings would be needed for effects from high Li⁺ concentration in LOW or low Li⁺ concentration in HIGH). GEN2 was provided as a baseline because this has been the electrolyte in previous sintered electrode full cell reports. 17,20 Note that relative to GEN2, PEAK had much higher capacity retention at increasing rates: 62 vs. 83% at C/ 5 (4.3 mA cm⁻²) and 38 vs. 58% at C/2.5 (8.6 mA cm⁻²), consistent with significant benefits of improving electrolyte conductivity for mitigating transport limitations in thick sintered electrodes.

As described earlier, another route to improve transport through the electrode microstructure is to provide directional porosity in the direction of the net flux of Li⁺ transport during charge/discharge. 22-24 Towards this end, the pores in the electrode microstructure for the thicker LTO electrode were aligned via ice-templating, also known as freeze-casting, and two of the electrolyte formulations had rate capability evaluation paired with ice-templated LTO electrodes (LCO electrodes for all cells used in this study were not icetemplated and were processed using the same methods/ processes). Details on the ice-templating process can be found in the ESI† and previous reports. 39-41 In previous studies, ice-templated LTO was found to improve the rate capability of sintered electrodes, consistent with mitigating the rate limiting Li⁺ mass transport processes.²² In that previous report, GEN2 was used as the electrolyte, and thus GEN2 electrolyte with an ice-templated electrolyte was evaluated (noted as GEN2_ICE). The other electrolyte evaluated with an ice-templated LTO anode was the one with the highest rate capability from earlier (PEAK, Fig. 2a), and this combination was referred to as PEAK_ICE. As shown in Fig. 2b, for both electrolytes the retention of capacity at increasing rates was greater for the ice-templated electrodes relative to those that did not have templated directional porosity (e.g., GEN2_ICE > GEN2 and PEAK_ICE > PEAK). This was consistent with previous results that ice-templated microstructures with aligned pores facilitated improved rate capability, which was interpreted in the context of improved ion transport through the electrode microstructure mitigating the limiting process in the electrochemical cell.²²

To further demonstrate the improvements of higher conductivity electrolytes and ice-templated microstructures for thick sintered electrode batteries, a Ragone plot of areal capacity dependence on areal current density during discharge for all cells used in this report is shown in Fig. 2c. This is the same cycling data as Fig. S2† with the rate and capacity on areal basis and mA/mA h outputs. The advantages of mitigated Li⁺ transport limitations through both ice-templating and a higher conductivity electrolyte (PEAK_ICE) relative to the baseline electrolyte with both electrodes processed via hydraulic pressing (GEN2) is apparent at increasing rates. For example, at 8.6 mA cm⁻² the discharge capacity of GEN2 was 5.9 mA h cm⁻², while the capacity of PEAK_ICE was 10.5 mA h cm⁻². Relative to other published results for high electrode loadings, 18,19,24,42-44 the cells in this report were relatively high in areal capacity

especially for current densities exceeding 5 mA cm⁻². While these results are encouraging, further efforts are ongoing to better understand the transport properties of electrolytes with multiple salts and the impacts of pore size and connectivity in addition to alignment in the microstructure.

Conclusions

In this work, batteries where both electrodes were thick sintered electrodes comprised of all electroactive materials were evaluated with regards to retention of capacity at increasing rate. Under the assumption that rate capability limitations were due to molecular transport limitations in the electrode microstructure, two design routes were pursued in isolation and combination: a higher conductivity electrolyte formulation and templated electrode microstructure with directional pore alignment. Both the higher conductivity electrolyte and the templated microstructure were found to improve rate capability, and the combination of both of these design improvements had the highest rate capability of the evaluated cells. This work demonstrated promising results in design strategies to enable higher rate capability for thick sintered electrode batteries, which is a key limitation that must be overcome for this high energy density strategy to have potential in applications that require even moderate rates relative to composite electrode Li-ion battery technology.

Conflicts of interest

No conflicts of interest are declared.

Acknowledgements

Funding is acknowledged from the National Science Foundation, grant CMMI-1825338 and CMMI-1825216. Nippon Shokubai Co., Ltd. is acknowledged for providing the LiFSI used in the electrolytes.

Notes and references

- 1 V. Etacheri, R. Marom, R. Elazari, G. Salitra and D. Aurbach, Energy Environ. Sci., 2011, 4, 3243-3262.
- 2 M. M. Thackeray, C. Wolverton and E. D. Isaacs, Energy Environ. Sci., 2012, 5, 7854-7863.
- 3 X. Ge, S. Liu, M. Qiao, Y. Du, Y. Li, J. Bao and X. Zhou, Angew. Chem., Int. Ed., 2019, 58, 14578-14583.
- 4 J. Liao, Y. Han, Z. Zhang, J. Xu, J. Li and X. Zhou, Energy Environ. Mater., 2021, 4, 178-200.
- 5 J. B. Goodenough and K. S. Park, J. Am. Chem. Soc., 2013, 135, 1167-1176.
- 6 N. Nitta, F. Wu, J. T. Lee and G. Yushin, Mater. Today, 2015, 18, 252-264.
- 7 H. Pan, S. Zhang, J. Chen, M. Gao, Y. Liu, T. Zhu and Y. Jiang, Mol. Syst. Des. Eng., 2018, 3, 748-803.
- 8 X. Zhou, L. J. Wan and Y. G. Guo, Adv. Mater., 2013, 25, 2152-2157.

Communication **MSDE**

- 9 K. Liu, Y. Liu, H. Zhu, X. Dong, Y. Wang, C. Wang and Y. Xia, Acta Phys.-Chim. Sin., 2020, 36, 1912030.
- 10 P. V. Braun and J. B. Cook, ACS Nano, 2018, 12, 3060-3064.
- 11 Y. Yamada, J. Wang, S. Ko, E. Watanabe and A. Yamada, Nat. Energy, 2019, 4, 269-280.
- 12 K. M. Diederichsen and B. D. McCloskey, Mol. Syst. Des. Eng., 2020, 5, 91-96.
- 13 H. Zheng, J. Li, X. Song, G. Liu and V. S. Battaglia, Electrochim. Acta, 2012, 71, 258-265.
- V. Murray, D. S. Hall and J. R. Dahn, J. Electrochem. Soc., 2019, 166, A329-A333.
- 15 T. Marks, S. Trussler, A. J. Smith, D. Xiong and J. R. Dahn, J. Electrochem. Soc., 2010, 158, A51-A57.
- 16 D. Kehrwald, P. R. Shearing, N. P. Brandon, P. K. Sinha and S. J. Harris, J. Electrochem. Soc., 2011, 158, A1393-A1399.
- 17 J. P. Robinson, J. J. Ruppert, H. Dong and G. M. Koenig, J. Appl. Electrochem., 2018, 48, 1297-1304.
- 18 W. Lai, C. K. Erdonmez, T. F. Marinis, C. K. Bjune, N. J. Dudney, F. Xu, R. Wartena and Y. M. Chiang, Adv. Mater., 2010, 22, E139-E144.
- 19 M. E. Sotomayor, C. de La Torre-Gamarra, B. Levenfeld, J. Y. Sanchez, A. Varez, G. T. Kim, A. Varzi and S. Passerini, J. Power Sources, 2019, 437, 226923.
- 20 Z. Nie, S. Ong, D. S. Hussey, J. M. LaManna, D. L. Jacobson and G. M. Koenig, Mol. Syst. Des. Eng., 2020, 5, 245-256.
- 21 K. X. Wang, X. H. Li and J. S. Chen, Adv. Mater., 2015, 27, 527-545.
- 22 Z. Nie, R. Parai, C. Cai, C. Michaelis, J. M. LaManna, D. Hussey, D. Jacobson, D. Ghosh and G. Koenig, J. Electrochem. Soc., 2021, 168, 060550.
- 23 L. Li, R. M. Erb, J. Wang, J. Wang and Y. M. Chiang, Adv. Energy Mater., 2019, 9, 1802472.
- 24 L. L. Lu, Y. Y. Lu, Z. J. Xiao, T. W. Zhang, F. Zhou, T. Ma, Y. Ni, H. B. Yao, S. H. Yu and Y. Cui, Adv. Mater., 2018, 30, 1706745.
- 25 E. R. Logan, D. S. Hall, M. M. Cormier, T. Taskovic, M. Bauer, I. Hamam, H. Hebecker, L. Molino and J. R. Dahn, J. Phys. Chem. C, 2020, 124, 12269-12280.

- 26 E. R. Logan, E. M. Tonita, K. L. Gering, J. Li, X. Ma, L. Y. Beaulieu and J. R. Dahn, J. Electrochem. Soc., 2018, 165, A21-A30.
- 27 E. R. Logan and J. R. Dahn, Trends Chem., 2020, 2, 354-366.
- 28 Z. Nie, P. McCormack, H. Z. Bilheux, J. C. Bilheux, J. P. Robinson, J. Nanda and G. M. Koenig Jr, J. Power Sources, 2019, 419, 127-136.
- 29 J. Neuhaus, E. von Harbou and H. Hasse, J. Power Sources, 2018, 394, 148-159.
- 30 C. L. Berhaut, D. Lemordant, P. Porion, L. Timperman, G. Schmidt and M. Anouti, RSC Adv., 2019, 9, 4599-4608.
- 31 Z. Zhang, Y. Du, Q. C. Wang, J. Xu, Y. N. Zhou, J. Bao, J. Shen and X. Zhou, Angew. Chem., Int. Ed., 2020, 59, 17504-17510.
- 32 A. Nyman, M. Behm and G. Lindbergh, Electrochim. Acta, 2008, 53, 6356-6365.
- 33 H. J. Kim, N. Voronina, H. Yashiro and S. T. Myung, ACS Appl. Mater. Interfaces, 2020, 12, 42723-42733.
- 34 H. B. Han, S. S. Zhou, D. J. Zhang, S. W. Feng, L. F. Li, K. Liu, W. F. Feng, J. Nie, H. Li, X. J. Huang and M. Armand, J. Power Sources, 2011, 196, 3623-3632.
- 35 Z. Qi and G. M. Koenig Jr, ChemistrySelect, 2016, 1, 3992–3999.
- 36 Z. Qi and G. M. Koenig Jr, J. Power Sources, 2016, 323,
- 37 G. Tuin, A. C. I. Peters, A. J. G. Van Diemen and H. N. Stein, J. Colloid Interface Sci., 1993, 158, 508-510.
- 38 D. Ghosh, N. Dhavale, M. Banda and H. Kang, Ceram. Int., 2016, 42, 16138-16147.
- 39 X. Zhang, Z. Ju, L. M. Housel, L. Wang, Y. Zhu, G. Singh, N. Sadique, K. J. Takeuchi, E. S. Takeuchi, A. C. Marschilok and G. Yu, Nano Lett., 2019, 19, 8255-8261.
- 40 S. Deville, J. Mater. Res. Technol., 2013, 28, 2202-2219.
- 41 R. Parai, T. Walters, J. Marin, S. Pagola, G. M. Koenig Jr and D. Ghosh, Materialia, 2020, 14, 100901.
- 42 X. Wu, S. Xia, Y. Huang, X. Hu, B. Yuan, S. Chen, Y. Yu and W. Liu, Adv. Funct. Mater., 2019, 29, 1903961.
- 43 X. Qin, X. Wang, J. Xie and L. Wen, J. Mater. Chem., 2011, 21, 12444-12448.
- 44 J. S. Sander, R. M. Erb, L. Li, A. Gurijala and Y. M. Chiang, Nat. Energy, 2016, 1, 1-7.